Zeitschrift für Physikalische Chemie Neue Folge, Bd. 155, S. 29–54 (1987)

NMR Quadrupole Relaxation of Xenon-131 in Water

A Molecular Dynamics Simulation Study

By Jürgen Schnitker* and Alfons Geiger**

Institut für Physikalische Chemie der RWTH Aachen,
Templergraben 59, 5100 Aachen, Federal Republic of Germany

Dedicated to Hermann Gerhard Hertz on the occasion of his 65th birthday

(Received May 25, 1987)

Molecular dynamics simulation / NMR quadrupole relaxation

An aqueous solution of ^{131}Xe at room temperature has been modeled in a molecular dynamics simulation of ST2 water with a Lennard-Jones solute. The electric field gradient fluctuation of purely electrostatic origin at the solute nucleus is investigated. Factors of static and dynamic screening are determined. The electric field gradient time correlation function does not decay monoexponentially, but shows contributions from various time domains in the range of 0.01 to 4.0 ps. The integrated correlation time is about 0.5 ps. The fluctuations are mainly caused by the molecules in the first hydration shell of the solute. The initial fast decay of the time correlation function is due to hindered translations and rotations as well as to a cooperative symmetry conservation of the hydration shell. The calculated relaxation rate is in good agreement with the experimental value.

Es wurde eine wäßrige ^{131}Xe-Lösung bei Zimmertemperatur mittels einer molekulardynamischen Simulationsrechnung untersucht und die Fluktuation des elektrischen Feldgradienten am Ort des gelösten Teilchens analysiert. Statische und dynamische Abschwächungsfaktoren wurden berechnet. Die Zeitkorrelationsfunktion des Feldgradienten zerfällt stark nichtexponentiell und enthält Beiträge unterschiedlicher Zeitskalen zwischen 0,01 und 4,0 ps. Die integrierte Korrelationszeit ergibt sich zu etwa 0,5 ps. Die Fluktuationen werden hauptsächlich durch die Moleküle der ersten Hydrathülle verursacht. Der schnelle Zerfall der Zeitkorrelationsfunktion bei kurzen Zeiten ergibt sich aus behinderten Translations- und Rotationsbewegungen wie auch durch kooperative Symmetricerhaltung in der Hydrathülle. Die berechnete Relaxationsrate stimmt mit den experimentellen Werten gut überein.

1. Introduction

Measurements of the nuclear magnetic relaxation of nuclei with spin quantum number $I > 1/2$ are widely employed for the investigation of the struc-

* *Present address:* Department of Chemistry, University of Texas, Austin, Texas 78712

** *Present address:* Physikalische Chemie, Fachbereich Chemie der Universität Dortmund, 4600 Dortmund, West Germany

ture and microdynamical behaviour of liquids. The relaxation of most of these nuclei is dominated by quadrupolar coupling, i.e. the interaction between the nuclear electric quadrupole moment and the fluctuating electric field gradient (efg) effective at the nuclear site [1]. The efg is due to the complete intra- and intermolecular charge distribution in the surroundings of the nucleus. In the case of atoms or monoatomic ions in solution the field gradient is of *inter*molecular origin and the fluctuations are caused by thermal motion of the solvent molecules.

There are two mechanisms for the energetic coupling between solute nucleus and solvent. On the one hand, there is a direct electrostatic interaction between solvent charges and the nuclear quadrupole moment; on the other hand, the field gradient can also be due to distortions of the symmetry of the electron cloud around the nucleus, which are induced, for example, by collisions with solvent molecules. Various models which attempt to elaborate on these mechanisms have been proposed in the last two and a half decades. Electronic distortion effects have been considered by Deverell [2] and Mishustin and Kessler [3]. The electrostatic theories can be divided into explicitly molecular models and continuum models. The *molecular* electrostatic approach is due to Hertz [4–6] and Valiev [7, 8] and has recently been reformulated by Versmold [9] on the basis of rigorous tensor algebra. A more graphical model has also been proposed by Friedman [10]. An electrostatic *continuum* model has been developed by Hynes and Wolynes [11] and was generalized recently by Stiles and Byrnes [12]. The electrostatic theories also account for electronic effects, but only in the sense of a constant electronic polarization, i.e. an overall multiplication of the field gradient with the so-called Sternheimer, or antishielding, factor [13, 14].

Out of these models, especially the relaxation theory of Hertz has been utilized very successfully to reproduce the experimental relaxation rates of many nuclei in many solvents [6]. The essential quantities, which determine the quadrupolar relaxation rate, are the mean square amplitude $\overline{V_{zz}^2}$ and the correlation time τ_c of the efg fluctuation. In the extreme narrowing case the corresponding relation is:

$$\frac{1}{T_1} \sim \overline{V_{zz}^2} \cdot \tau_c . \tag{1}$$

In several cases it has been possible to perform relaxation time measurements in so-called non-extreme narrowing situations [15, 16], where it is possible to determine these two quantities separately. The observed magnitude of τ_c is compatible with the electrostatic, but *not* with the electronic theories [16]. Electronic relaxation mechanisms may be important for special systems, like liquid noble gases, but for polar solvents the electrostatic approach is most promising.

Even the latest electrostatic theories [9, 12] leave open many questions about the details of the relaxation process. Computer simulations offer the possibility to observe and analyze model systems directly on a molecular level. Several Monte Carlo (MC) [17–19] and molecular dynamics (MD) [20–22] simulations of this kind have been performed recently. While the MC method yields only the mean square fluctuation $\overline{V_{zz}^2}$, with MD simulations it is possible to determine the correlation time τ_c as well. The latter method thus permits, in principle, an "ab initio" calculation of the relaxation rate $1/T_1$.

We report here a molecular dynamics simulation of an aqueous solution of ^{131}Xe. Natural Xenon contains this isotope with an abundance of 21%. ^{131}Xe has a spin quantum number of $I = 3/2$ and hence a nuclear electric quadrupole moment. Measurements of the relaxation rate of this nucleus in various solvents, including water, have been published recently [23–25]. The "Xenon in water" system is of special interest in the context of hydrophobic hydration [26–29]. In living systems Xenon acts as an anesthetic and NMR spectroscopy of this element can be used as a probe in the investigation of membranes, protein suspensions etc. [29]. Our simulated system consists of 215 ST2 water molecules [30] and a Xenon atom, which interacts with the solvent via a Lennard-Jones pair potential. It has been shown repeatedly that the hydration of nonpolar solutes can be simulated successfully with this model [28, 31–33]. The simulation extends over 39 ps. We calculate the efg tensor at the solute site that is due to the partial charges of all ST2 molecules. The mean tensor squared yields $\overline{V_{zz}^2}$ and from the corresponding time correlation function (tcf) we obtain τ_c. When calculating the relaxation rate $1/T_1$, we correct for the electronic polarization effects by multiplication with a Sternheimer factor. Thus we differ from the recent MD simulation of Engström *et al.* [22]. These authors have investigated the efg fluctuation in aqueous ionic solutions; however, they determined the field gradient from parameterized ab initio calculations. In this strict quantum mechanical approach electronic and electrostatic contributions are treated in a unified, but also indistinguishable, manner. From our procedure, however, we expect an explicit answer about the applicability of electrostatic approaches. By calculating a variety of time averages and tcfs we attempt to get a more detailed insight into the molecular motions governing the relaxation mechanism.

We start with a description of the simulated system and the efg calculations (Secs. 2 and 3). The results are presented and discussed in Sec. 4. We focus on the statics and dynamics of the field gradient fluctuation and compare the computed relaxation rate with experimental values. We also investigate the underlying molecular motions and look at the field gradient fluctuation in the V-structure of water. In the final Sec. 5 the simulation results are compared with the predictions of various relaxation models.

2. Simulation outline

Our system setup essentially corresponds to the previous study [28]. 215 ST2 water molecules [30] and a Lennard-Jones sphere of mass 131 amu are confined to a cubic box under standard toroidal boundary conditions. The density is 1.03 g cm^{-3}. The Eqs. of motion are integrated in the Verlet form [34] with a time step of $1.22 \cdot 10^{-15}$ s, using the constrained algorithm SHAKE for the water molecules [35]. The water-water interactions are calculated with a spherical cut-off of 7.8 Å, using an instantaneous reaction field and a tapering function smoothing the discontinuity at the cut-off [36]. Due to the use of the latter, excellent energy conservation without any need for velocity rescaling is achieved. The Lennard-Jones parameters for the solute-water interaction (which is calculated in the minimum image convention) are derived from experimental values for the Xe-Xe-interaction [37] and the corresponding ST2 parameters. By using the arithmetic and geometric mean, one obtains $\sigma = 3.7$ Å and $\varepsilon = 0.18$ kcal/mol, respectively.

After introduction of the solute into an equilibrated water configuration, a simulation of 32000 time steps was performed on a VAX-11/780 with an attached FPS-164 processor. For the last 18000 time steps, equivalent to 22 ps, configurations were recorded and analyzed. The mean kinetic temperature is 295 K. The corresponding value for the weakly interacting dissolved particle is 284 K and hence close to the solvent temperature.

3. Computation of electric field gradients

Each of the 215 ST2 molecules gives rise to an efg tensor $\mathbf{V}^i$ at the solute site. The cartesian components are

$$V^i_{\alpha\beta} = \frac{\partial^2 U^i}{\partial\alpha\,\partial\beta}, \quad i = 1\ldots215; \quad \alpha,\beta = x,y,z \tag{2}$$

with U^i being the Coulomb potential produced by the four partial charges q^i_j of the ST2 model:

$$q^i_j = \pm 0.2357\,\mathrm{e}, \quad j = 1\ldots4.$$

We note that these charges have been used as pure fitting parameters in the formulation of the ST2 model [30]. Therefore the ST2 dipole moment is 2.35 Debye, larger than the dipole moment of the isolated water molecule, but close to the mean dipole moment in the liquid [38].

By summing over all molecules in the simulation cell, we obtain the total field gradient tensor

$$\mathbf{V} = \sum_{i=1}^{N} \mathbf{V}^i, \quad N = 215. \tag{3}$$

The ensemble averaged tcf of this quantity can be calculated from its cartesian components

$$\langle \mathbf{V}(0):\mathbf{V}(t)\rangle = \sum_{\alpha,\beta} \langle V_{\alpha\beta}(0)\cdot V_{\alpha\beta}(t)\rangle . \tag{4}$$

Nuclear quadrupolar relaxation is determined by the spectral density of this tcf [1]. If the Larmor frequency of the NMR experiment is small compared to the characteristic frequency of the efg fluctuations, i.e. in the extreme narrowing case, only the zero frequency value of the spectral density enters and Eq. (1) is obtained [39] with the correlation time

$$\tau_c \equiv \int_0^\infty \frac{\langle \mathbf{V}(0):\mathbf{V}(t)\rangle}{\langle \mathbf{V}(0):\mathbf{V}(0)\rangle} dt . \tag{5}$$

For the mean square fluctuation amplitude, given by the value of the tcf at time zero, we use the notation of Friedman [10]:

$$\overline{V_{zz}} = \left\langle \frac{2}{3}\mathbf{V}(0):\mathbf{V}(0)\right\rangle^{1/2} \tag{6}$$

which yields

$$\overline{V_{zz}}^2 = \left\langle q^2\left(1+\frac{\eta^2}{3}\right)\right\rangle \tag{7}$$

if the field gradient tensor is evaluated in a molecule fixed principle axes system [40]. q denotes the element of the diagonalized tensor with the largest absolute value and η is an asymmetry parameter

$$\eta \equiv \frac{V'_{xx}-V'_{yy}}{V'_{zz}} \tag{8}$$

with $|q \equiv V_{zz}| \geq |V_{yy}| \geq |V_{xx}|$.

We note that we compute the tcf (4) and the mean square fluctuation (6) by strictly accounting for all components of the tensor as shown on the right hand side of Eq. (4). This is superior to the method of Engström *et al.* who confined themselves to only one [17–19] or three [22] of the diagonal components in the laboratory system. Because of the symmetry and vanishing trace of the efg tensor, statistical deviations in single components of the tensor cancel partly if summed up according to Eq. (4) [21]. Thus our approach yields higher accuracy for the mean square fluctuation $\overline{V_{zz}}^2$ as well as for the correlation time τ_c.

Inserting sum (3) into Eq. (4) the tcf of the total field gradient can be decomposed into sums over self- and cross-correlation functions of single particle field gradients

$$\langle \mathbf{V}(0):\mathbf{V}(t)\rangle = \sum_i \langle \mathbf{V}^i(0):\mathbf{V}^i(t)\rangle + \sum_{i\neq j}\sum \langle \mathbf{V}^i(0):\mathbf{V}^j(t)\rangle . \tag{9}$$

In an analogous fashion to Eqs. (4) and (6), one defines the tcf

$$\langle \mathbf{V}^{(1)}(0) : \mathbf{V}^{(1)}(t) \rangle \equiv \sum_i \langle \mathbf{V}^i(0) : \mathbf{V}^i(t) \rangle \tag{10a}$$

with the corresponding correlation time

$$\tau_c^{(1)} \equiv \int_0^\infty \frac{\langle \mathbf{V}^{(1)}(0) : \mathbf{V}^{(1)}(t) \rangle}{\langle \mathbf{V}^{(1)}(0) : \mathbf{V}^{(1)}(0) \rangle} dt \tag{11}$$

and the mean fluctuation amplitude

$$\overline{V_{zz}^{(1)}} \equiv \left\langle \frac{2}{3} V^{(1)}(0) : V^{(1)}(0) \right\rangle^{1/2} \tag{12}$$

to characterize the *single particle* field gradient. In Eq. (12) the field gradient contribution of each single molecule is squared before the sum is evaluated and hence mutual quenching of the sign affected single particle contributions does not occur. Therefore, a comparison of the numerical results of (6) and (12) yields information about the static many particle correlations (*static* screening factor). Analogously, a *dynamic* screening factor can be defined using the correlation times (5) and (11). The difference between the total field gradient tcf (9) and the self correlation function (10a) yields the cross correlation function

$$\langle \mathbf{V}^{(1)}(0) : \mathbf{V}^{(2)}(t) \rangle \equiv \sum_{i \neq j} \sum \langle \mathbf{V}^i(0) : \mathbf{V}^j(t) \rangle . \tag{10b}$$

Note that the tcfs (10a) and (10b), which we denote self- and cross-correlation functions of single particle field gradients, are in fact two- and three-particle correlation functions [9] because of the dependence on the solute position.

Care has to be taken in the computation of the single particle tcf (10a) because of the periodic boundary conditions involved in the simulation technique. To use the minimum image (MI) shifted positions of the solvent molecules with respect to the solute at any instant – which is acceptable for the computation of the total field gradient (4) – would mean to include trajectories which contain "jumps" from one box side to the other if an MI boundary is crossed by a solvent molecule. A proper remedy is the replication of the original box, so that the particle trajectories no longer extend on the surface of a four-dimensional torus, but in principle in the infinite (but periodic) three-dimensional space. This is achieved by tracing the particle trajectories in time without applying MI-shifts. The tcf (10a) has been calculated by this method, once using only the trajectories of the molecules in the original box, and alternatively applying the same procedure to the molecules of a new system of $3 \cdot 3 \cdot 3 = 27$ original boxes. We find good agreement between the results of these two approaches. However,

the first discussed naive approach, including MI-shifts, yields markedly different single particle tcfs.

4. Results

From the amplitude (Sec. 4.1) and the correlation time (Sec. 4.2) of the efg fluctuation, we get the relaxation rate (Sec. 4.3), which is compared with experimental values. In Secs. 4.4, 4.5, and 4.6 we exploit the typical advantage of computer experiments to be able to analyze molecular processes in detail.

4.1. Mean square fluctuation of the electric field gradient

By including all 215 molecules around the solute the mean square fluctuation $\overline{V_{zz}^2}$ (6) comes out to $(0.55 \pm 0.07) \cdot 10^{39}\ V^2/m^4$ [41]. Fig. 1 shows the convergence of this value when more and more neighbors are included

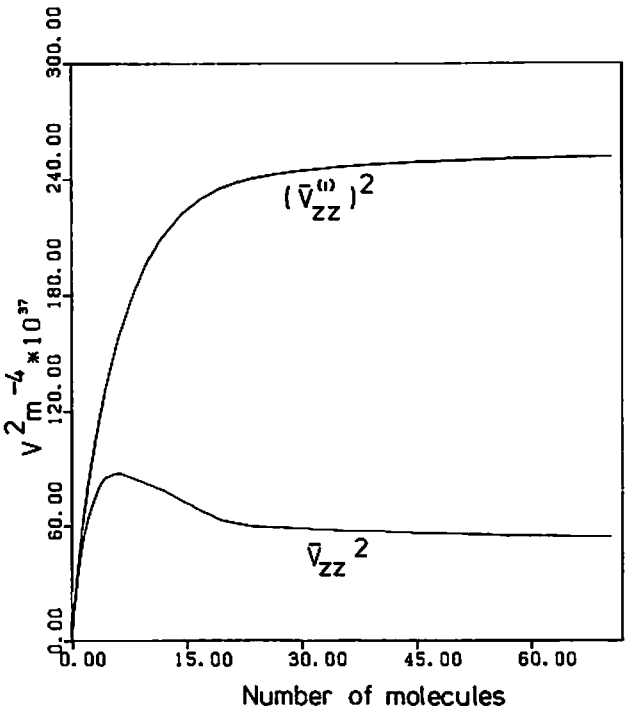

Fig. 1. Mean square fluctuation of the efg if an increasing number of nearest neighbors is included in the efg evaluation. Squaring after (lower curve, usual definition) or before (upper curve, screening eliminated) summation of the single particle contributions.

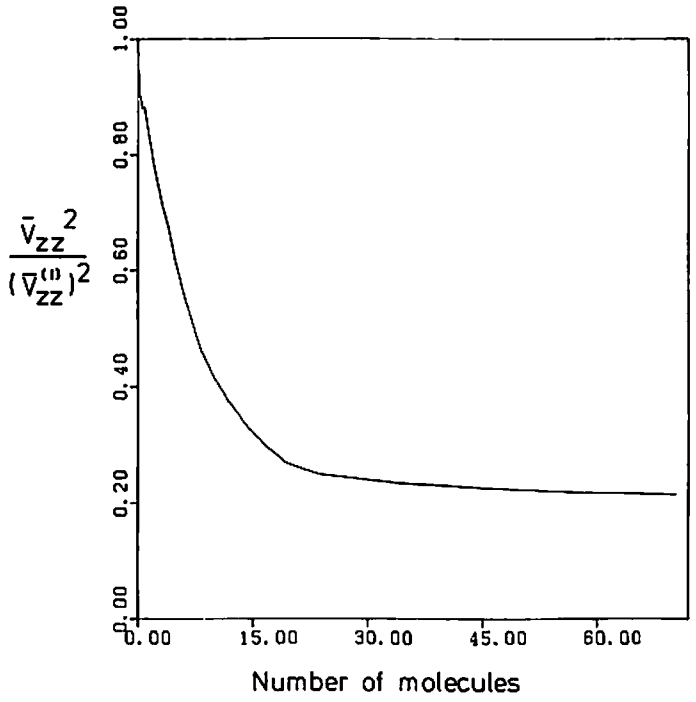

Fig. 2. Quotient of quantities from Fig. 1.

into spherical shells around the solute (lower line). The curve exhibits a maximum at six neighbors, equivalent to 4 Å, which coincides with the first maximum in the computed Xenon-oxygen radial pair correlation function [28]. A fairly close approach to the limiting value is reached at about 20 neighbors which compares with the first minimum in the pair correlation function at 5.5 Å or 21.5 neighbors. Consequently, the overwhelming part of the efg at the solute nucleus can be assigned to the molecules in the first hydration shell.

Fig. 1 demonstrates also the convergence behavior of the quantity (12) where the order of summing and squaring has been exchanged and hence the mutual quenching of contributions from different molecules is eliminated (upper line). The converged value including all molecules comes out to $(\overline{V_{zz}^{(1)}})^2 = 2.54 \cdot 10^{39}\ \mathrm{V^2 m^{-4}}$. For comparison, the average mean square field gradient produced by the closest water molecule is $0.45 \cdot 10^{39}\ \mathrm{V^2 m^{-4}}$.

The quotient of both curves from Fig. 1 is a measure of the mutual quenching of the efg due to many-particle correlations. This function which displays "screening" in an integrated way is shown in Fig. 2. Up to about ten neighbors screening increases roughly linear with the number of molecules.

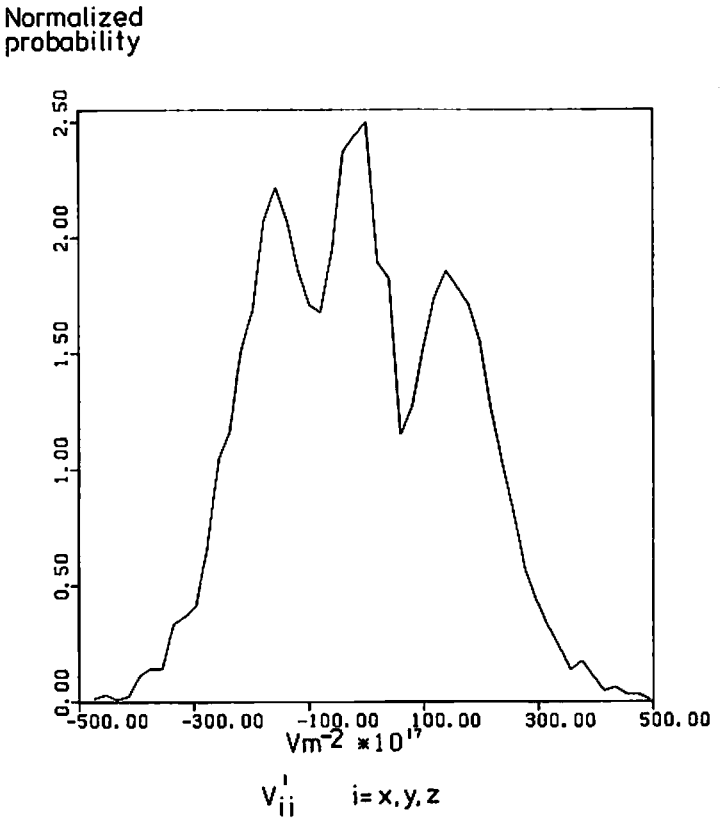

Fig. 3. Distribution of components in the principal axes system of the efg tensor.

Beyond about 20 neighbors an asymptotic limit is approached quickly. The limit value, which we denote as the static screening factor f_{stat}, coincides with the square of the so-called polarization factor P [5, 13], which has been discussed frequently [9, 11, 19]. We obtain $f_{stat} = 0.22$ and hence $P = (f_{stat})^{1/2} = 0.47$.

By diagonalization of the efg tensor, three statistically equivalent tensor components in the principle axes system are obtained. Their distribution over the observed field gradient range is given in Fig. 3. Apart from the main peak in the middle it shows another unexpected peak at a nonvanishing field gradient, together with its symmetric counterpart. The mean square fluctuation in the principle axes system may be characterized completely by the two parameters q and η according to Eq. (7). We find $\langle q^2 \rangle = 0.49 \cdot 10^{39}\ V^2m^{-4}$, i.e. a value less than the actual mean square fluctuation specified previously. Accordingly, the asymmetry parameter comes out to a nonvanishing value of $\langle \eta \rangle = 0.60$.

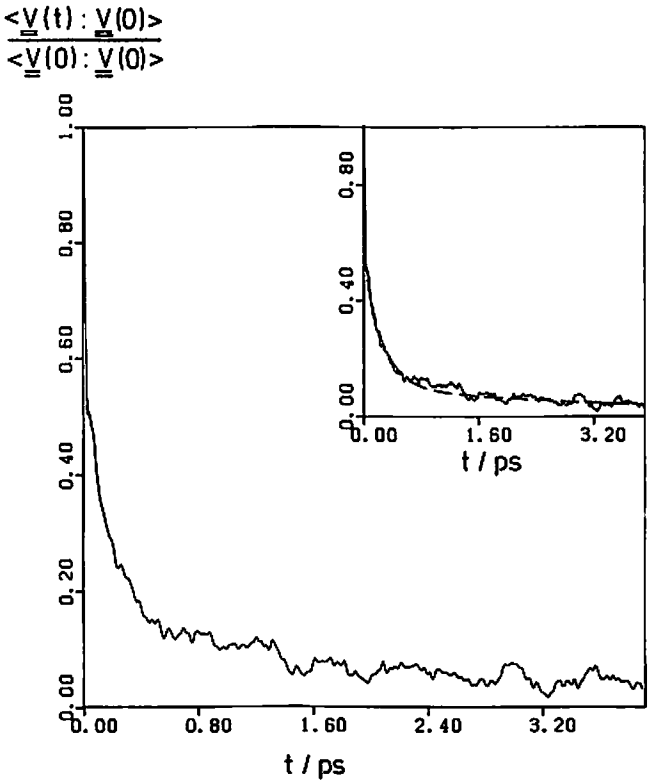

Fig. 4. Normalized tcf for efg fluctuation in aqueous Xenon solution. Inset: Fit with sum of three exponentials.

4.2. Electric field gradient time correlation function

The obtained tcf (4) displayed in Fig. 4 shows the same overall pattern as observed in the simulation of ions in water [22]. A very rapid initial decay on a time scale of a fraction of a picosecond is followed by a slower decay on a picosecond time scale. Careful inspection shows that at least three time domains can be distinguished. A good fit involving three exponentials with $\tau = 0.01$ ps (weight 0.45), 0.25 ps (weight 0.45) and 4.0 ps (weight 0.1) is displayed in the inset of Fig. 4. For the present, we consider this fit as a first unbiased attempt to quantify the decay of the field gradient tcf in a phenomenological way. Later we will discuss the physical mechanisms that can be associated with the time domains of the above shown fit.

The integral over the tcf up to infinity is the decisive dynamical quantity in an NMR experiment in the extreme narrowing regime [Eqs. (1) and (5)]. By direct integration up to 3.9 ps and using the fit given above for the range beyond, we find $\tau_c = 0.54$ ps. Another measure for the time evolution of

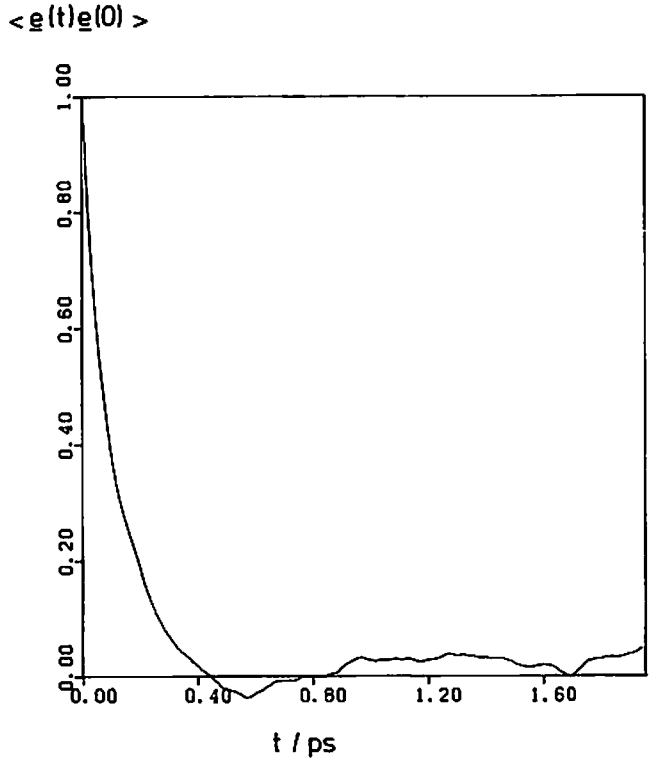

Fig. 5. Reorientational tcf for the principal axes (unit vectors) of the efg tensor.

the field gradient tensor is the reorientational behavior of the principal axes [see Eqs. (7) and (8)]. The corresponding tcf is shown in Fig. 5 and again an initial rapid decay in a fraction of a picosecond is observed. Obviously, the principal axes system changes drastically in connection with small lateral displacements of hydration shell water molecules.

4.3. Relaxation rate

With the two quantities $\overline{V_{zz}}^2$ and τ_c at hand we can calculate the NMR relaxation rate which is given by

$$\frac{1}{T_1} = \frac{3}{40}\frac{2I+3}{I^2(2I-1)}\left(\frac{eQ(1+\gamma_\infty)}{\hbar}\right)^2 \overline{V_{zz}}^2 \tau_c \,. \tag{13}$$

The spin quantum number for ^{131}Xe is $I = 3/2$ and for the nuclear electric quadrupole moment a value of $Q = -0.12 \cdot 10^{-24}$ cm^{-2} is generally used,

the uncertainty specified with ± 10% [42]. The Sternheimer factor $(1+\gamma_\infty)$ is not known accurately as is common for this quantity. Tentatively, we make use of two values given recently [43] and thus obtain the following relaxation rates:

$$1/T_1 = 191\ s^{-1} \text{ with } (1+\gamma_\infty) = 139 \text{ [43a]}$$

$$1/T_1 = 246\ s^{-1} \text{ with } (1+\gamma_\infty) = 158 \text{ [43b]}.$$

Stengle *et al.* [25] determined the relaxation rate of ^{131}Xe in H_2O and in D_2O at 25°C from line width measurements to be $1/T_1 = 179\ s^{-1}$ and $251\ s^{-1}$, respectively. Mazitov *et al.* [24] report values of 147 ± 7 and $180 \pm 9\ s^{-1}$, respectively. The measurements had been carried out at the low concentrations given by the saturation solubility of Xenon at the applied moderate pressures. No concentration dependence could be observed [25].

The proximity to our computed relaxation rates is remarkable in view of the simplifications which have entered into the model and the uncertainty in the numerical values of the employed constants.

4.4. Single particle electric field gradient

The self- and cross-correlation functions (10a) and (10b) of the single particle field gradients are displayed in Fig. 6, along with the corresponding tcf for the total field gradient discussed previously (lowest line). Whereas the *normalized* self and cross tcf show a similar behavior, a distinct difference to the total field gradient tcf is visible. It is important to realize that the zero time values of these three tcfs are very different. The mean square fluctuation values, given in section 4.1. are equivalent to

$$\langle V(0):V(0)\rangle = 0.83 \cdot 10^{39}\ V^2/m^4,$$

$$\langle V^{(1)}(0):V^{(1)}(0)\rangle = 3.81 \cdot 10^{39}\ V^2/m^4$$

and hence yield a *negative* sign of the cross-tcfs (notice the factor 3/2):

$$\langle V^{(1)}(0):V^{(2)}(0)\rangle = -2.98\ V^2/m^4.$$

This is another manifestation of strong efg quenching. It is clearly the near cancellation between the oppositely signed self- and cross-tcfs that leads to the marked short time decay of the total efg correlation function.

For the single particle self-tcf we estimate the correlation time $\tau_c^{(1)}$, i.e. the integral up to infinity, to be about 3.4 ps. Together with the total field gradient correlation time of 0.54 ps given above, we may calculate a dynamic screening factor by defining $f_{dyn} = \tau_c/\tau_c^{(1)}$ and obtain $f_{dyn} = 0.16$.

Keyes and Kivelson [44] argued that in ordinary liquids the correlation time τ_{col} of a collective orientation dependent variable can be related to the

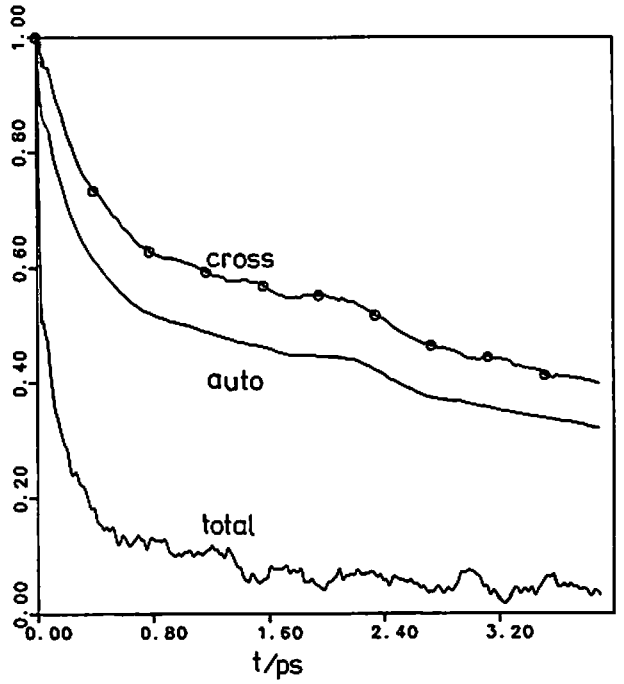

Fig. 6. Solid line and solid line with circles: Normalized single particle tcfs for efg auto-correlations and efg cross-correlations, respectively. Lowest line: Normalized tcf of total efg tensor as in Fig. 4.

correlation time τ_{sing}, which describes the fluctuation of the individual constituents, by

$$\tau_{col} = \frac{g_2}{j_2}\tau_{sing} \,. \tag{14}$$

g_2 and j_2 are static and dynamic correlation factors, respectively, and g_2 is in our case identical with f_{stat}. Usually it is assumed that $j_2 \approx 1$ and therefore $f_{dyn} \approx f_{stat}$, which is in excellent accordance with our observations. However, it should be kept in mind that the derivation of Keyes and Kivelson refers to exponentially decaying single particle and collective tcfs, which are clearly not found in our simulation. Our results also show that for rather *long times* the single particle and collective tcfs decay with about equal time constants: $\tau'_{col} \approx \tau'_{sing}$.

4.5. Molecular motions

Even within an entirely electrostatic framework it is not at all clear what kinds of molecular motion are predominantly responsible for the efg fluc-

tuation. We try to address this question by calculating tcfs for the translational and rotational motion of both the solute and the solvent molecules. Since it has been shown that the region beyond the first hydration shell does not significantly contribute to the field gradient, only the molecules of the first hydration shell need to be considered. The residence time of the molecules within the shell then specifies an upper limit for the time scale of possibly contributing motions.

We compute single particle tcfs of the hydration shell molecules by applying a procedure proposed by Impey *et al.* [45] and average only over those particles, which satisfy the following requirements: The particle has to be inside the first hydration shell at both times $t = t'$ and $t = t' + \Delta t$ and may not have left the shell for any continuous period longer than t^* in the meantime (the reference time t' runs over the whole analysis interval). With the introduction of the parameter t^* the problem arising from those molecules which temporarily leave the first hydration shell can be handled in a well defined manner. The limiting values for t^* are the time resolution of the analyzed configurations on the one hand and the total time of the analyzed simulation interval on the other hand. In our case these limits are 0.01 ps and 22 ps, respectively; and the first hydration shell extends up to 5.5 Å with a mean of 21.5 solvent molecules in it. Within the 22 ps analysis interval 58 of the total of 215 water molecules reside at one time or another within this shell.

For the simplest single particle property "residence/nonresidence", described by a function $f(t) = 1$ or 0, the tcfs of Fig. 7 are obtained with the dashed lines referring to the limiting values for t^*. Impey *et al.* [45] used exclusively $t^* = 2$ ps (solid line). It can be seen that the residence tcf for this value is very close to the tcf obtained with the upper limit value. Integrating the solid line up to infinity with an appropriate exponential continuation yields a lifetime for the solvent molecules in the first hydration shell of about 8.2 ps. This value is of the same order of magnitude or larger than most of the correlation times which are typically used in the description of the microdynamics in water and aqueous solutions. In particular the Debye correlation time τ_1, which is for pure water at room temperature about 8 ps, is still within that range. (The situation is different for structure breaking ions which have considerably smaller hydration shell molecule lifetimes.)

The outlined method can now be applied to the computation of other single particle tcfs of hydration shell molecules. We present results for $t^* = 2$ ps but the tcfs discussed below are quite insensitive to any t^* value. Fig. 8 displays in the inset the tcf of the relative velocity between the center of mass of the hydration shell water molecules and the Xenon atom. This figure also shows the power spectrum, which is obtained by Fourier transformation over the time range shown in the inset. We discuss the position of various peaks in terms of characteristic fluctuation times $\tau =$

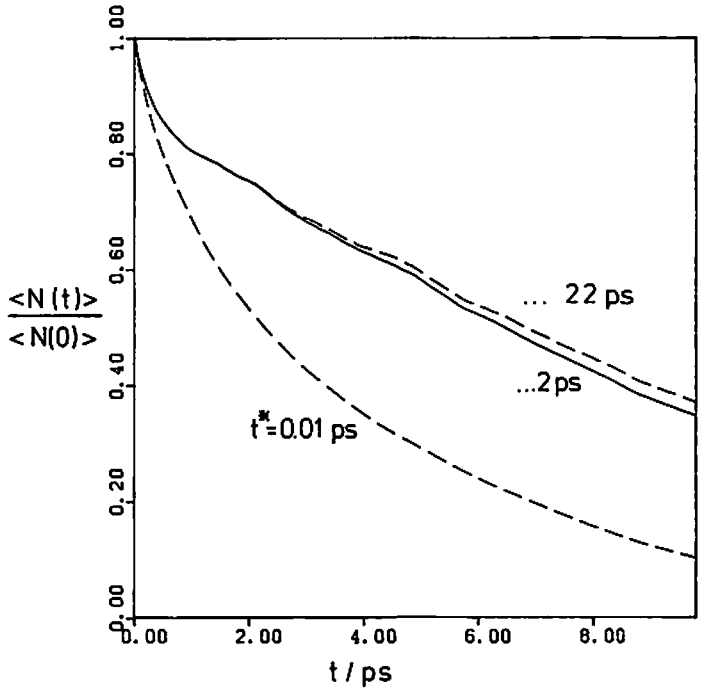

Fig. 7. Normalized residence tcf of water molecules in first hydration shell of Xenon. Parameter t^* refers to maximum time interval molecules are allowed to leave hydration shell without being neglected.

$2\,\pi/\omega$. Naturally the relative motion must reflect contributions from both partners. The two peaks at $\tau = 0.6$ ps and 0.15 ps are the dominant peaks of the single particle velocity tcf of the water molecules [30]. These time domains are usually assigned to two specific kinds of hindered translation of the water molecules. The high frequency motion with $\tau = 0.15$ ps is assumed to be due to intermolecular vibrations between hydrogen bonded molecules. The low frequency motion with $\tau = 0.6$ ps is assigned to the movement of the reference particle within the "cage" formed by the surrounding molecules. In another picture, O–O–O bond angle oscillations are assumed to be responsible [46].

The highest peak at 1.5 ps stems from the Xenon motion: due to its relatively slow motion in a wide cage, the power spectrum consists of one broad asymmetric band, positioned at the corresponding frequency (not shown here). As we will discuss later, the influence of this very pronounced motional contribution clearly shows up in the single particle field gradient tcf. We note here that the discussed fluctuation times belong to an intermediate scale if we consider the time scale of the field gradient tcf (Fig. 4).

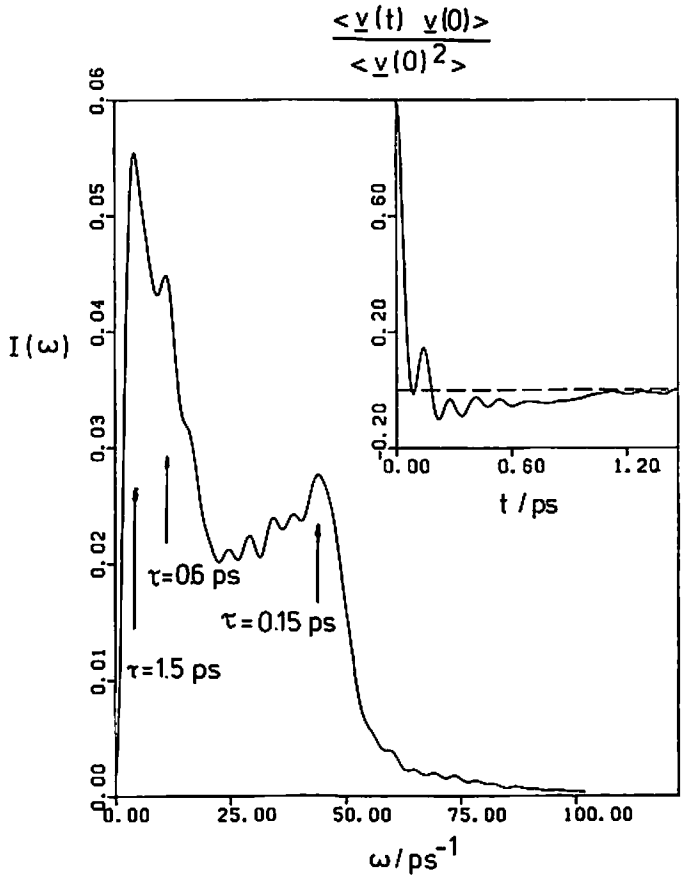

Fig. 8. Normalized tcf (inset) and corresponding power spectrum (main diagram) for relative velocity between center of mass of water molecules and Xenon nucleus.

Next we look at the translational and rotational motion directly (Fig. 9). According to the symmetry of the system, the translational motion is decomposed into a "lateral" and a radial component. The first part refers to the surface of spheres laid around the solute and is described by the reorientation of the connecting vector between the solute and the center of mass of the solvent molecule. For ideally radially oriented point dipoles the field gradient tcf refers to the decay of the second Legendre polynomial of this vector [4, 9] (plain curve of Fig. 9a). With respect to the radial component of the translational motion, the inverse of the fourth power of the radial distance enters into the field gradient in the point dipole picture. No hydration shell definition is required and the averaging can be performed over all molecule trajectories of the system (full curve with

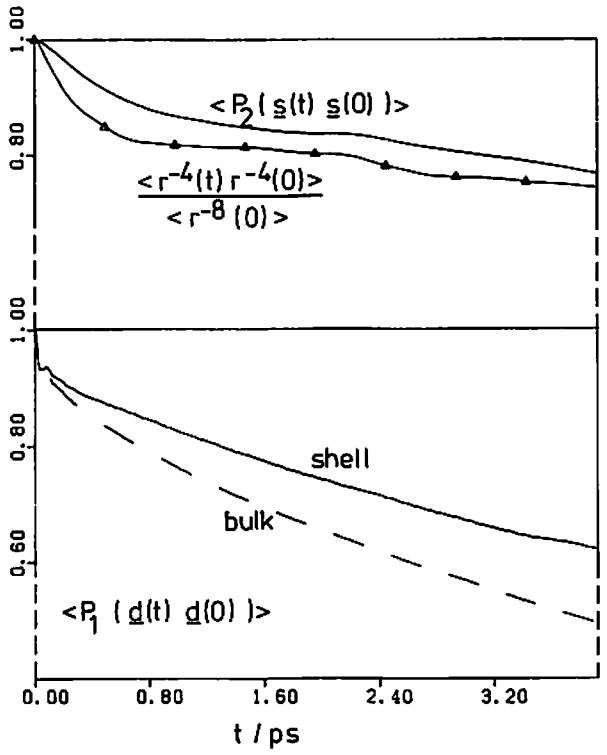

Fig. 9. Upper diagram, solid line: Reorientational tcf for second Legendre polynomial of the solvent center of mass to Xenon connecting vector ("lateral" translation of hydration shell molecules). Solid line within triangles: Translational tcf for radial motion of solvent center of mass relative to Xenon nucleus. — Lower diagram, solid line: Reorientational tcf for first Legendre polynomial of solvent dipole vectors in first hydration shell. Dashed line: Same tcf for bulk water molecules.

triangles). To calculate the influence of the pure rotation of the solvent molecules, the point dipole approximation is used again. It has been shown that the appropriate tcf refers to the decay of the first Legendre polynomial of the electric dipole vector [4] (plain curve of Fig. 9b). For the purpose of comparison, the corresponding correlation function for bulk water is also displayed (dashed curve). A pronounced structure making effect of the solute is clearly visible.

Assuming independence of the investigated motions and using the point dipole approximation, we can calculate the single particle field gradient tcf by multiplying the three translational and rotational tcfs from Fig. 9. The result is shown in Fig. 10 (plain curve). The dashed curve is the actual single particle field gradient decay already shown in Fig. 6. The full curve with

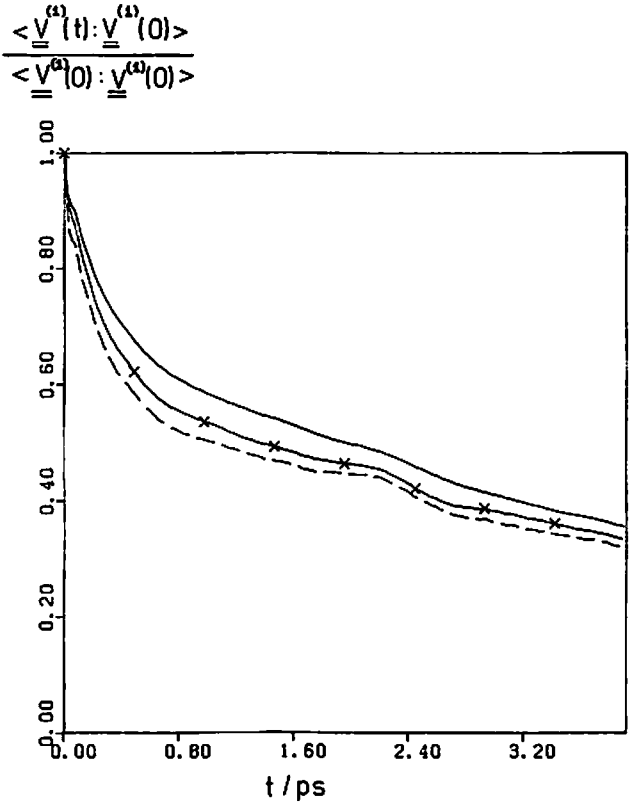

Fig. 10. Solid line: Normalized tcf obtained from multiplication of the three tcfs from Fig. 9 that refer to lateral displacement, radial translation, and internal rotation of hydration shell molecules. Dashed line: Single particle tcf for efg auto-correlations as in Fig. 6. Solid line with crosses: Single particle tcf for efg auto-correlations if only point dipolar part of ST2 charge distribution is considered.

the crosses is the computed single particle field gradient tcf if only the point dipole part of the ST2 charge distribution, positioned at the center-of-mass, contributes to the field gradient. The agreement of the three curves is satisfactory. The slight shift downwards while proceeding from the point dipole field gradient to the actual one is understandable. For higher multipole moments the internal rotation is described by Legendre polynomials which are of higher order than unity and hence decrease faster.

Concerning Figs. 9 and 10, the direct influence of two distinct types of motion on the single particle field gradient tcf can be conceived immediately. Hindered rotations, the so-called "librations" of the water molecules, lead to the rapid initial decay in Fig. 9b, which one finds likewise in Fig. 10. The bump-like feature of the field gradient tcf between 1.0 and 2.5 ps also

shows up in the distance tcf of Fig. 9a and becomes even more prominent, if one calculates the correlation function of the fluctuations around the average Xenon-water distance for every water molecule trajectory (not shown). An obvious explanation for the occurrence of this bump is the oscillation of the solute within its hydration cage, which leads to the prominent peak at $\tau = 1.5$ ps in the power spectrum Fig. 8.

4.6. Electric field gradient for the water V-structure

An interesting point of view of the microdynamics of water and aqueous solutions has been provided by Eisenberg and Kauzmann [47], who distinguished between the I-, V- and D-structures of liquid water, where the initials stand for "instantaneous", "vibrational" and "diffusional". The I-structure corresponds to the configurations obtained directly from a molecular dynamics simulation. The V-structure disregards local translation and rotational vibrations and is the structure actually probed with many experimental methods, e.g. IR spectroscopy. Hirata and Rossky introduced a realization of the V-structure for ST2 water into computer simulation [48]. Technically, all molecule positions are averaged over a certain number of configurations in the six-dimensional space formed by the cartesian center of mass coordinates and three Euler angles. Application of this method to the problem of the efg fluctuation is of interest as certain parts of the microdynamical motion may be suppressed.

In Fig. 11a we display tcfs for the total and single particle field gradient which are obtained with two choices of the averaging time. The solid lines refer to the I-structure and hence no averaging, the widely dashed lines in the middle refer to an averaging time of $\bar{\tau} = 0.1$ ps and the upper dashed lines to $\bar{\tau} = 0.2$ ps.

With the smaller averaging time the librations are suppressed and the rapid initial decay of both kinds of tcfs disappears. With the larger averaging time the broad translational high frequency band of Fig. 8 is also eliminated and the tcfs move further upwards. The integral up to infinity of the total field gradient tcf is roughly doubled at this point. Vice versa, we can conclude that the inclusion of hindered rotations and of the high frequency part of the hindered translations associated with hydrogen bond stretching reduces the correlation time by a factor of two.

The mean square fluctuations of the total field gradient are reduced to 79% with $\bar{\tau} = 0.1$ ps and 61% with $\bar{\tau} = 0.2$ ps, respectively, of the I-structure value. This is understandable as we observe a continuous narrowing of the water-Xenon radial pair correlation functions while proceeding from the I-structure to the V-structures. Obviously about 40% of the mean square fluctuation is due to the temporal approach of charge centers towards the solute nucleus during the vibrational periods of hindered rotations and fast hindered translations.

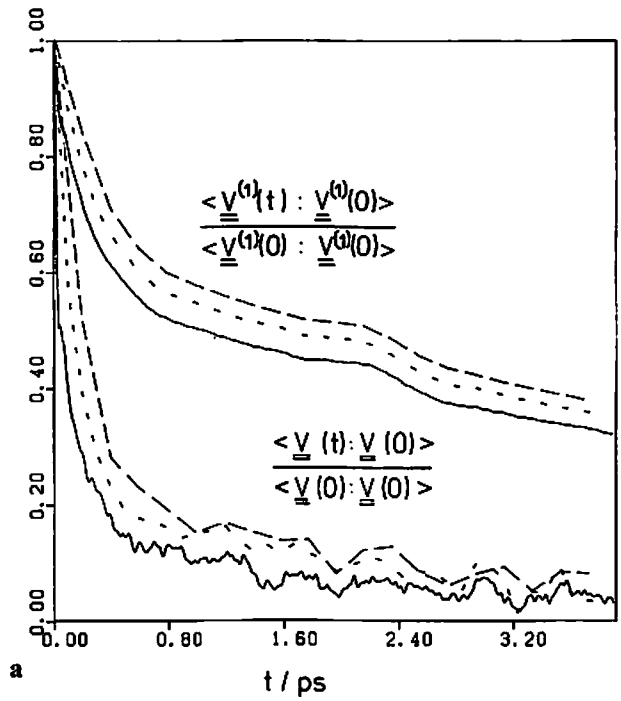

Fig. 11. a) Normalized tcfs of total efg tensor (three lower lines) and single particle efg tensor (auto-correlations, three upper lines) for Xenon in I-structure of water (solid lines), in V-structure with time averaging over $\bar{\tau} = 0.1$ ps (widely dashed lines), or in V-structure with time averaging over $\bar{\tau} = 0.2$ ps (narrowly dashed lines).

Fig. 11 b is the analog of Fig. 6 for a V-structure that is obtained with the extreme averaging interval of $\bar{\tau} = 1$ ps. Referring to our discussion in the previous section, all hindered translational and rotational motions of the water molecules should be averaged out under these conditions; but nevertheless the relative difference between the normalized tcfs persists.

This means that the presence of hindered motions is not really necessary to obtain the dynamic screening or "acceleration" effect that characterizes the fluctuation of the total field gradient relative to the single particle fluctuation. The retarded decay of the cross correlations evidently reflects a partial conservation of the hydration shell symmetry. We note that not only hindered motion but also the free solvent rotation does not effectively disrupt the overall symmetry pattern of the hydration shell. Consequently, a pronounced dynamic screening has to be expected. Only the much slower unhindered translational motion gives rise to a net degradation of the hydration shell symmetry.

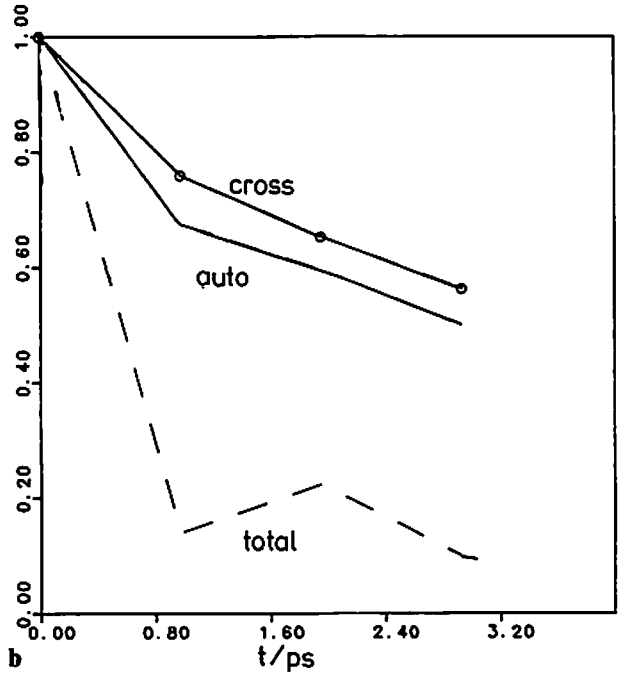

Fig. 11. b) Normalized tcfs for fluctuation of total efg tensor (dashed line) and single particle auto- and cross-correlations (solid line and solid line with circles respectively) in the V-structure of water with time averaging over $\bar{\tau} = 1$ ps.

5. Discussion

In Sec. 4.3 it was demonstrated that the experimentally measured relaxation rate of ^{131}Xe in water can be reproduced successfully by a simulation that is based on an entirely electrostatic approach. Considering the wealth of structural and thermodynamical simulation data that have elsewhere been compared with experimental evidence [28], this agreement is not likely to be fortuitous. It is now of interest to inquire whether any of the known electrostatic relaxation theories can account for the simulation results. This question is especially intriguing as we are able to compare separately the mean square amplitude and the correlation time of the efg fluctuation.

The results of such a comparison, carried out with formulas and parameters as given in the Appendix, are collected in Table 1. We consider the FRD ("fully random distribution") and NOS ("non-oriented solvation") versions of Hertz's microscopic electrostatic theory [6], the continuum theory of Hynes and Wolynes [11], and the generalized continuum theory of Stiles and Byrnes [12]. For completeness, we note that we do not discuss the theories of Friedman [10] and Valiev [8] because they are rather specific for the solvation structure of charged (ionic) solutes. The same restriction

Table 1. NMR relaxation of ^{131}Xe in water from simulation, electrostatic theories, and experiment.

	Simulation	Hertz theory Ref. [4–6]		Continuum theory Ref. [11, 12]		Experiment Ref. [25]
		FRD	NOS	Simple	Generalized	
$\frac{\overline{V_{zz}}^2}{10^{39}\,V^2m^{-4}}$	0.55	0.36	0.84	0.12	0.04	
$\frac{\tau_c}{ps}$	0.54	9		0.12		
$\frac{1/T_1}{s^{-1}}$	246	2660	6310	12	4	179

applies to the FOS ("fully oriented solvation") version of the theory of Hertz [6]. Another theory by Valiev [7], after all, is largely comparable with Hertz's theory and is not considered here either.

Inspection of Table 1 suggests that the Hertz theory gives roughly the right mean square amplitude of the efg fluctuation and that the continuum theory is better in the prediction of the fluctuation dynamics. The relaxation rate, however, is off by an order of magnitude in either case. The predictions would be better if parameters are chosen in ways similar to those in previous presentations of the models. Thus, the Hertz theory is usually implemented with the gas phase value for the water dipole moment (1.84 D) whereas we have here chosen the dipole moment of the ST2 model (2.35 D) which should actually be close to the effective value in the condensed phase [38]. Furthermore, the relaxation rates of the Hertz theory are usually calculated with a correlation time of $\tau_c = 2.5$ ps, which is the correlation time for the intramolecular proton-proton relaxation of the water molecule [5]. Our value of $\tau_c = 9$ ps, the Debye correlation time τ_1 for the solvation shell molecules, refers to the internal solvent rotation as the relevant dynamical process in the original formulation of the theory (decay of first order Legendre polynomials [4]). It is also possible to include a translational contribution in the sense of [5]

$$\frac{1}{\tau_c} = \frac{1}{\tau_1} + \frac{1}{\tau^*} \tag{15}$$

where τ_1 is again the Debye correlation time and τ^* refers to the translational motion of molecules on the periphery of shells laid around the solute ("lateral displacement"). From our simulation (Fig. 9) we can estimate $\tau^* \approx 20$ ps and hence obtain a total correlation time τ_c of about 6 ps and a reduction of the relaxation rate by about 30%. Finally, it should be mentioned that the continuum theory prediction of the relaxation rate is much better if the bare atom radius is used to characterize the penetration

range of the dielectric continuum [11, 12]. Naturally, only a rough upper estimate for the relaxation rate can be calculated in this way.

Surprisingly, the polarization factor determined in the simulation ($P = 0.47$) almost agrees with the value of $P = 0.41$ that is calculated with the simple continuum formula of Cohen and Reif [13]:

$$P = \frac{3 + 2\,\varepsilon_0}{5\,\varepsilon_0}. \tag{16}$$

It has been shown, however, that the derivation of this formula does not really apply to the kinds of systems considered here [19]. The enormous difficulties of a proper analytical calculation of the polarization factor have been emphasized, and quick progress in this endeavor is not expected [11]. Hertz sets $P = 0.5$ in an ad hoc fashion which thus appears to be a good choice [5].

Dynamic screening effects are neglected in the microscopic electrostatic theory by assuming identical temporal decay of the two and three particle correlations [5]. This assumption does not hold true (Fig. 6). Although the difference in the correlation times is not very large, the decay of the summed field gradient tensor is strongly affected because of the opposite sign of auto and cross correlations. The continuum theory, on the other hand, implicitly accounts for static and dynamic screening within its very formalism [11, 12], but both effects are obviously overemphasized (Table 1). Another lack of all proposed theories is the complete neglect of hindered motions. From the results presented above it is sufficiently clear that some account for the oscillatory microdynamics is essential for a proper understanding of the efg fluctuation.

In conclusion, molecular dynamics simulation has shown that the NMR quadrupole relaxation of ^{131}Xe in water can be adequately described with a model of simple electrostatic effects. A precise microdynamical understanding of the field gradient fluctuation is now beginning to emerge. Most important, our analysis elucidates the intricate nature of static and dynamic screening effects. Such effects were not yet considered consistently in the pioneering microscopic theory of Hertz [4, 5] and appear to be substantially overestimated in the electrostatic continuum theory [11, 12]. Recently, Versmold [9] was able to derive some important functional properties of the field gradient tcf for certain idealized solvation structures. A comprehensive reformulation of the microscopic electrostatic theory in the spirit of such a rigorous treatment appears to be called for.

Acknowledgement

We thank Prof. Peter J. Rossky, Austin, for providing the V-structure program. Financial support of the Fonds der Chemischen Industrie is gratefully acknowledged.

Appendix

For clearness, we subsequently give the explicit formulas and the numerical values used in the preparation of Table 1.

Hertz FRD model [6]

$$\overline{V_{zz}}^2 = \frac{16\pi c}{r_0^5} P^2 \left(\frac{\mu}{4\pi\varepsilon_0}\right)^2 \tag{A1}$$

$$\tau_c = \tau_1 . \tag{A2}$$

Hertz NOS model [6], including FRD contribution from molecules outside of first hydration shell

$$\overline{V_{zz}}^2 = \left(\frac{20\, n_s}{r_s^2} + \frac{16\pi c}{r_2^5}\right) P^2 \left(\frac{\mu}{4\pi\varepsilon_0}\right)^2 . \tag{A3}$$

Correlation time as Eq. (A2).

Continuum model [11, 12]

$$\overline{V_{zz}}^2 = \frac{200\, kT}{a^5} \frac{(\varepsilon_r^0 - \varepsilon_r^\infty)}{4\pi\varepsilon_0 (2 + 3\varepsilon_r^0)(2 + 3\varepsilon_r^\infty)} \tag{A4}$$

$$\tau_c = \frac{2 + 3\varepsilon_r^\infty}{2 + 3\varepsilon_r^0} \tau_1 . \tag{A5}$$

Generalized continuum model [12]

The mean square fluctuation from the simple continuum model, Eq. (A4), has to be multiplied with the factor

$$\left(1 - \frac{1 + \gamma + \frac{1}{3}\gamma^2}{1 + \gamma + \frac{9}{20}\gamma^2 + \frac{7}{60}\gamma^3 + \frac{1}{60}\gamma^4}\right) \tag{A6}$$

where

$$\gamma = \frac{a}{(D\tau_1)^{1/2}} . \tag{A6'}$$

Correlation times as Eq. (A5).

From the set up of our system, we have automatically for the solvent concentration $c = 0.0334\ \text{Å}^{-3}$, for the solvent dipole moment $\mu = 2.353$ D, and for the high frequency permittivity $\varepsilon_r^\infty = 1$ (non-polarizable water model). From the simulation, we find for the solvent temperature $T = 295$ K, for the polarization factor $P = 0.47$, for the static permittivity $\varepsilon_r^0 = 123$ (see Ref. [49] for appropriate calculation under reaction field conditions), for the rotational correlation time of the first shell molecules $\tau_1 = 9$ ps, and for the self diffusion coefficient $D = 2.3 \cdot 10^{-5}\ \text{cm}^2\ \text{s}^{-1}$ [28]. The radii a_0, r_0, r_s, and r_2 are not unambiguously defined, but the following choices appear to be reasonable: $a_0 = 3.3$ Å from the first passage through $g(r) = 1.0$ of the solute-ST2 charge center radial pair correlation functions, $r_0 = 3.5$ Å from the first passage through $g(r) = 1.0$ of the solute-oxygen pair correlation function, $r_s = 3.95$ Å and $r_2 = 5.5$ Å from the first maximum and

first minimum, respectively, of the latter. The number of first shell molecules is $n_s = 21.5$.The relaxation rates in Table 1 are calculated with the nuclear constants $I = 3/2$, $Q = -0.12 \cdot 10^{-24}$ cm^2 [42], and $(1 + \gamma_\infty) = 158$ [43b].

References

1. A. Abragam, *The Principles of Nuclear Magnetism* (Clarendon, Oxford, 1961), Chapter VIII.
2. C. Deverell, Mol. Phys. **16** (1969) 491.
3. A. I. Mishustin and Yu. M. Kessler, J. Solution Chem. **4** (1975) 779.
4. H. G. Hertz, Z. Elektrochem. **65** (1961) 20.
5. H. G. Hertz, Ber. Bunsenges. Phys. Chem. **77** (1973) 531.
6. H. Weingärtner and H. G. Hertz, Ber. Bunsenges. Phys. Chem. **81** (1977) 1204.
7. K. A. Valiev, Sov. Phys. JETP **37** (1959) 77.
8. K. A. Valiev and B. M. Khabibullin, Russ. J. Phys. Chem. **35** (1961) 1118.
9. H. Versmold, Mol. Phys. **57** (1986) 201.
10. H. L. Friedman, in: *Protons and Ions Involved in Fast Dynamics Phenomena*, ed. P. Laszlo, p. 27. Elsevier Amsterdam, 1978.
11. J. T. Hynes and P. G. Wolynes, J. Chem. Phys. **75** (1981) 395. For an important error correction see Ref. [12].
12. P. J. Stiles and G. B. Byrnes, Chem. Phys. **100** (1985) 217.
13. M. H. Cohen and F. Reif, Solid State Phys. **5** (1957) 321.
14. R. M. Sternheimer, Phys. Rev. **146** (1966) 140.
15. A. Geiger and H. G. Hertz, Adv. Mol. Relax. Proc. **9** (1976) 293.
16. H. Weingärtner, J. Magn. Res. **41** (1980) 74.
17. S. Engström, Thesis, Lund 1980.
18. S. Engström and B. Jönsson, Mol. Phys. **43** (1981) 1235.
19. S. Engström, B. Jönsson and B. Jönsson, J. Magn. Reson. **50** (1982) 1.
20. A. Geiger, Habilitationsschrift, Karlsruhe 1981.
21. J. Schnitker, Diplomarbeit, Aachen 1982.
22. S. Engström, B. Jönsson and R. W. Impey, J. Chem. Phys. **80** (1984) 5481.
23. T. R. Stengle, N. V. Reo and K. L. Williamson, J. Phys. Chem. **85** (1981) 3772.
24. R. K. Mazitov, H. G. Hertz, V. F. Garanin, K. M. Endikeev, A. V. Ilyasov and V. F. Sukhoverkhov, Dokl. Akad. Nauk SSSR **273**(1) (1983) 131.
25. T. R. Stengle, N. V. Reo and S. K. L. Williamson, J. Phys. Chem. **88** (1984) 3225; N. V. Reo, Thesis, Amherst, Massachusetts 1984.
26. W. Kauzmann, Adv. Protein Chem. **14** (1959) 1.
27. H. G. Hertz, Ber. Bunsenges. Phys. Chem. **68** (1964) 907.
28. A. Geiger, Ber. Bunsenges. Phys. Chem. **85** (1981) 52.
29. T. R. Stengle, S. M. Hosseini, H. G. Basiri and K. L. Williamson, J. Solution Chem. **13** (1984) 779; K. W. Miller, N. V. Reo, A. J. M. Schoot Uiterkamp, D. P. Stengle and K. L. Williamson, Proc. Nat. Acad. Sci. USA **78** (1981) 4946.
30. F. H. Stillinger and A. Rahman, J. Chem. Phys. **60** (1974) 1545.
31. A. Geiger, A. Rahman and F. H. Stillinger, J. Chem. Phys. **70** (1979) 263.
32. C. Pangali, M. Rao and B. J. Berne, J. Chem. Phys. **71** (1979) 2982.
33. D. A. Zichi and P. J. Rossky, J. Chem. Phys. **83** (1985) 797.
34. L. Verlet, Phys. Rev. **159** (1967) 98.
35. J.-P. Ryckaert, G. Ciccotti and H. J. C. Berendsen, J. Comput. Phys. **23** (1977) 327.
36. O. Steinhauser, Mol. Phys. **45** (1982) 335.
37. H.-L. Lin and R. L. Robinson, J. Chem. Phys. **54** (1971) 52.
38. F. H. Stillinger, in: *The liquid state of matter*, ed. E. W. Montroll and J. L. Lebowitz, p. 341. North Holland, Amsterdam, 1982.

39. Note that for nuclei with spin $I \geq 1$ a relaxation rate $1/T_1$ is defined only in the extreme narrowing case: P. S. Hubbard, J. Chem. Phys. **53** (1970) 985.
40. Note that the quantity $\langle V_{zz}^2 \rangle$ used in Ref. [17–19] is related by $\langle V_{zz}^2 \rangle = \langle \overline{V_{zz}}^2/5 \rangle$.
41. Standard deviation of the mean as estimated from subaverages over first and second half of simulation.
42. W. L. Faust and N. N. McDermott, Phys. Rev. **123** (1961) 198.
43. a) M. R. Keenan, L. W. Buxton, E. J. Campbell, T. J. Balle and W. H. Flygare, J. Chem. Phys. **73** (1980) 3523; b) F. A. Baiocchi, T. A. Dixon, C. H. Joyner and W. Klemperer, J. Chem. Phys. **75** (1981) 2041.
44. T. Keyes and D. Kivelson, J. Chem. Phys. **56** (1972) 1057.
45. R. W. Impey, P. A. Madden and I. R. McDonald, J. Phys. Chem. **87** (1983) 5071.
46. M. G. Sceats, M. Stavola and S. A. Rice, J. Chem. Phys. **70** (1979) 3927.
47. D. Eisenberg and W. Kauzmann, *The Structure and Properties of Water*, Oxford University Press, New York 1969, Chap. 4.
48. F. Hirata and P. J. Rossky, J. Chem. Phys. **74** (1981) 6867.
49. O. Steinhauser, Chem. Phys. **79** (1983) 465.